

Shear wave anisotropy beneath the Tibetan Plateau

Daniel E. McNamara and Thomas J. Owens

Department of Geological Sciences, University of South Carolina, Columbia

Paul G. Silver

Department of Terrestrial Magnetism, Carnegie Institution of Washington, Washington D.C.

Frances T. Wu

Department of Geological Sciences, State University of New York at Binghamton

Abstract. Eleven broadband digital seismic stations were deployed across the central Tibetan Plateau in the first extensive passive-source experiment attempted within the Tibetan Plateau. One year of recording resulted in 186 event-station pairs which we analyze to determine the characteristics of shear wave splitting in the upper mantle beneath the array. Measurements of the fast polarization direction (ϕ) and delay time (δt) for *SKS* and direct *S* arrivals reveal systematic variations along the north-south oriented array. In the north central region of the plateau, very large delay times are observed at three stations, the largest of which is BUDO with $\delta t=2.4$ s. However, at TUNL, which is off the northern edge of the plateau and 110 km from BUDO, and at sites in the south central plateau, δt decreases by nearly a factor of 3. We also observe a systematic rotation of ϕ from about 45° (NE) to 90° (E-W) from south to north along the array. A previously identified zone of inefficient *Sn* propagation correlates well with our region of large δt observations. The large delay times suggest that a relatively high number of anisotropic crystals are preferentially aligned within the mantle-lid, beneath the north central portion of the Tibetan Plateau. In most cases, fast polarization directions appear to be parallel to surface geologic features suggesting as much as 200 km of the upper mantle has been involved in the collisional deformation that has produced the Tibetan Plateau.

Introduction

Constraining the evolution of the lithospheric mantle during the collision of India and Eurasia is critical to choosing between deformational models of continent-continent collision zones. Part of the problem in developing sufficient seismic constraints on the upper mantle beneath the Tibetan Plateau derives from the fact that it is very difficult to develop high-resolution models of the lithospheric mantle in general. This problem has been compounded in the Tibetan Plateau by severe physiographic and political limitations on access to the region. We recently were afforded the opportunity to address the issue of access through a cooperative Sino-American research program. In this paper, we implement the technique of *Silver and Chan* [1991] to extract estimates of shear wave velocity anisotropy from well-recorded *SKS* and direct *S* wave data collected within the Tibetan Plateau. There is increasing evidence that velocity anisotropy is related to finite strain in the upper mantle [Hess, 1964; Nicolas and Christensen, 1987; Silver and Chan, 1991]. Our goal is to constrain Tibetan Plateau tectonic models based on the nature of strain in the upper mantle inferred from measurements of shear wave splitting.

In a cooperative research program conducted by the University of South Carolina, State University of New York at Binghamton,

and the Institute of Geophysics, State Seismological Bureau, China, 11 three-component, digital seismic stations were deployed across the central Tibetan Plateau (Figure 1 and Table A1¹). The 700 km-long, central portion of the array follows the Qinghai-Tibet Highway. At each array site, except TUNL, there was a Reftek 72A-02 data logger and a broadband Streckeisen STS-2 sensor. The STS-2 is an active feedback seismometer and has corner frequencies of 1/120 Hz and 50 Hz. A Gurupl CMG-3ESP seismometer, with corner frequencies of 1/30 Hz and 30 Hz, was installed at TUNL. This was the first extensive passive-source experiment attempted within the Tibetan Plateau. In one year of operation (July 1991 to July 1992), 614 events were recorded and identified using the U. S. Geological Survey (USGS) monthly Preliminary Determination of Epicenters (PDE) catalog, and 366 of them are teleseismic ($\Delta > 30^\circ$). Data at 10 stations were recorded in both a 40 sample/s event triggered stream and a 1 sample/s continuous stream. Because of cultural noise causing excessive triggering at LHASA, a 5 sample/s continuous data stream was used to ensure recording of adequate teleseismic data. All stations were operational for at least 90% of the year of deployment except for GANZ and XIGA [Owens *et al.*, 1993a]. Both GANZ and XIGA were down as much as 40% of the year for a variety of reasons including vandalism. Trigger parameters, array performance, and site construction constraints are described by Owens *et al.* (1993a).

¹Appendix Tables A1-A3 are available with entire article on microfiche. Order from American Geophysical Union, 2000 Florida Avenue, N.W., Washington DC, 20009. Document number B94-001; \$2.50. Payment must accompany order.

Copyright 1994 by the American Geophysical Union.

Paper number 93JB03406.
0148-0227/94/93JB-03406\$05.00

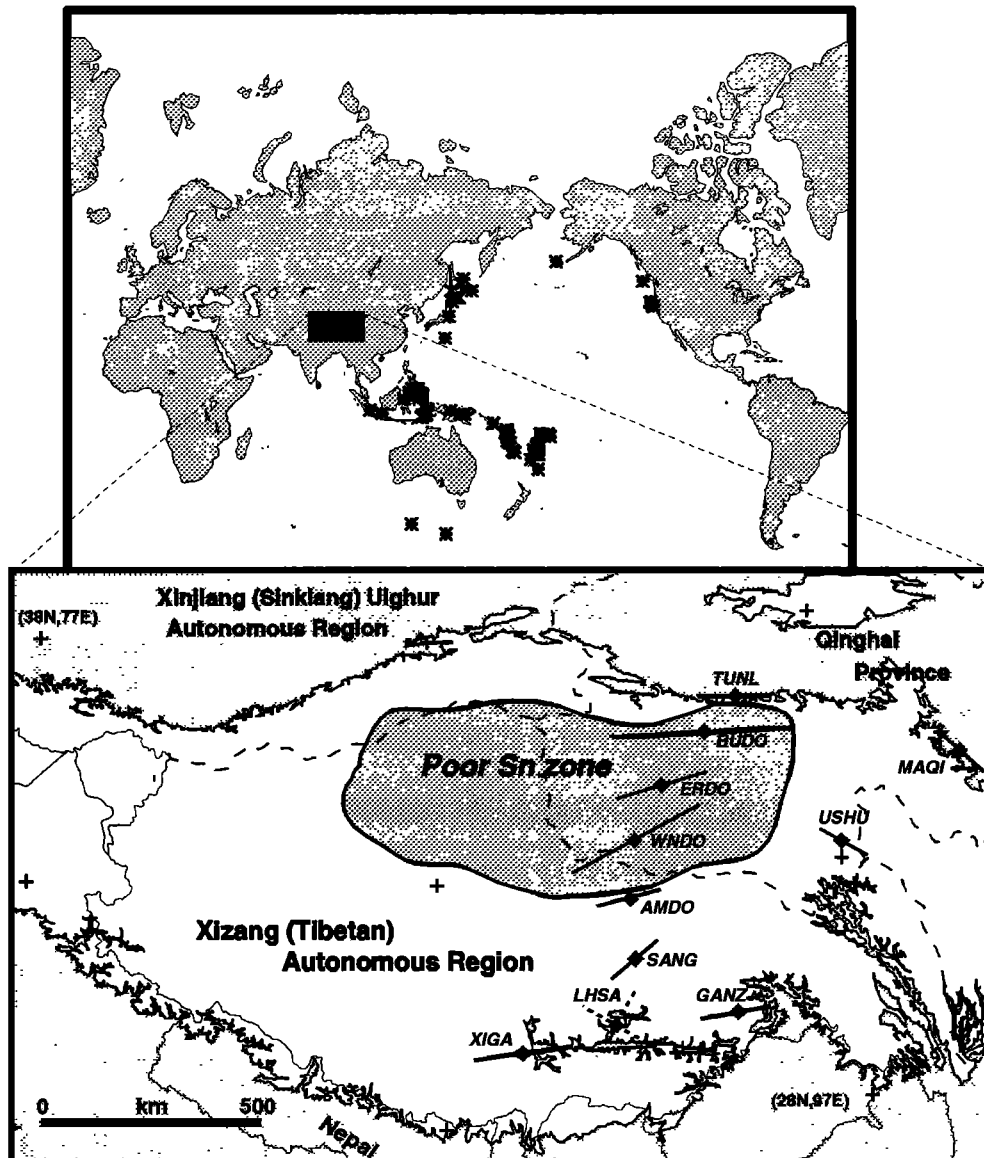


Figure 1. 1991-1992 Tibetan Plateau seismic experiment base map. (top) The panel shows the distribution of events (solid stars) used in this study and the location of the array on the Tibetan Plateau (dark shaded rectangle). (bottom) The panel shows the locations of experiment stations (solid diamonds) with resultant anisotropy parameters plotted as lines (ϕ , δt) at each station. The orientation of the lines corresponds to ϕ , and relative δt is shown by the length of the line. The dashed lines at LHSA indicate the null directions. The open area is above the 4000 m contour, including the Tibetan Plateau. The area labeled "poor S_n zone" is a zone of inefficient S_n propagation identified by *Ni and Barazangi* [1983].

In this study, we are interested in well-recorded teleseismic shear phases. We used 48 teleseismic events with impulsive SKS and direct S wave arrivals to examine anisotropy beneath the Tibetan Plateau (Table A2). Our primary source regions for the SKS arrivals were the active Fiji, Tonga, and Vanuatu regions and the less active region of western North America. At teleseismic distances of 85° to 105° , the first shear wave arrival is the SKS phase. At epicentral distances of 40° to 75° the S wave is the principle shear arrival. Earthquakes with focal depths greater than 50 km are used to assure that S is well isolated from shear depth phases (sS , pS , $sSKS$). Source regions for the direct S wave are the active subduction zones of the western Pacific rim. Figure 1 shows the distribution of events recorded by the array and used in this study. Comprehensive

information on event and station locations, seismometer calibration, and timing issues are described in the experiment data report [Owens *et al.*, 1993b]. Station and event information are also available as microfiche tables. Event and station names used here are the same as those used in the data report.

The SKS phase leaves the source as an S wave, converts to a P wave as it travels through the outer core, and, finally, from the core-mantle boundary to the surface, it propagates again as an S wave. The P to S conversion at the core-mantle boundary causes the final leg of the SKS path to be radially polarized. Thus any observed shear wave splitting in the steeply incident SKS wave reflects anisotropy directly beneath the recording station, between the surface and the core-mantle boundary. Splitting between the horizontal components of S , with steep

incident angles beneath the receiver, also provides an excellent means for studying anisotropy beneath the receiver if proper care is taken to avoid source-side anisotropy [Kaneshima and Silver, 1992; Ozalaybey and Savage, 1994; Silver and Savage, 1993].

Tibetan Plateau Tectonic History, Geology, and Geophysics

The Tibetan Plateau is among the world's most impressive physiographic features from both an aesthetic and a scientific viewpoint. Surrounded by a majority of the world's tallest mountains and with an average elevation of 5000 m, the Tibetan Plateau inspires many questions about its geologic history. Many investigators have attempted to explain its anomalous characteristics using a wide variety of geologic and geophysical techniques, but few have had the opportunity to venture onto the plateau itself for direct sampling. Using earthquakes from the Tibetan Plateau, recorded outside the plateau at regional and teleseismic distances, investigators have placed first-order constraints on the geologic and geophysical nature of the region (see Molnar [1988] for a review).

The Tibetan Plateau extends from the south side of the Kunlun Shan to the north side of the Himalaya Range and consists of a series of micro-continental fragments that accreted onto the southern margin of Eurasia after the breakup of Gondwana [Dewey *et al.*, 1988; Windley, 1988]. The accretion of northward drifting fragments from the breakup of Gondwana terminated during the Tertiary with the collision of the Indian continental block. This collision is responsible for nearly 2000 km of convergence which gave rise to the anomalous peak elevations in the Himalaya and Karakoram ranges as well as the elevation and thickened crust of the Tibetan Plateau [Molnar, 1988; Tapponnier *et al.*, 1990; Harrison *et al.*, 1992; Dewey *et al.*, 1988].

Several models have been proposed to explain the anomalously thick crust of the Tibetan Plateau. Each falls into one of the two basic theories that describe the mechanism of uplift: (1) uplift occurred by shallow underthrusting of the Indian lithosphere beneath Eurasia at a late stage in the collision [Argand, 1924; Beghoul *et al.*, 1993]; (2) crustal thickening and lithospheric shortening occurred in response to compression generated from continental collision between the Indian and Eurasian plates [Dewey and Burke, 1973]. While both of these ideas can account for the thickness of the crust, distinct differences arise in the expected nature of the upper mantle. These simplistic versions of both classes of models have been modified in various ways to account for both evidence of a warm, thin lithosphere in the north central Tibetan Plateau and the relatively uniform uplift of the plateau [see Molnar, 1988].

Recent seismic investigations have produced results supporting both theories of uplift. Using earthquake travel times for paths crossing the plateau, Barazangi and Ni [1982] and Ni and Barazangi [1983] found high P_n and S_n velocities of 8.43 km/s and 4.73 km/s, respectively, within the Tibetan Plateau. They also found that S_n propagates efficiently in the upper mantle beneath most of Tibet but is severely attenuated in north central Tibet (Figure 1). They conclude that efficient propagation and high velocities are evidence that the Indian continental shield is underthrusting the Tibetan Plateau. In contrast, from a similar study, Chen and Molnar [1981] found relatively slower P_n and S_n velocities of 8.1 km/s and 4.7 km/s, respectively,

beneath the Tibetan Plateau. Molnar and Chen [1984] also found that $S-P$ travel time residuals were positive and much larger under the Tibetan Plateau than under the Himalayas, indicating low S wave velocities under the plateau. Molnar and Chen concluded that their results are more compatible with the crustal thickening theory of uplift than underthrusting. Based on S wave residuals, Molnar and Chen [1984] argued that there must be a thin (20-30 km) mantle lid beneath the Tibetan Plateau. Brandon and Romanowicz [1986] also present evidence for a thin lithosphere (100 km) beneath the north central Tibetan Plateau, using Rayleigh wave dispersion models. Using waveforms from Tibetan Plateau earthquakes, Zhou *et al.*, [1991] modeled a positive velocity gradient in the crust and a thin (60 km) relatively low velocity (8.29 km/s) mantle lid. The key to placing further constraints on Tibetan Plateau tectonics is understanding the anomalous nature of the upper mantle.

Analysis Procedures

Measurements of shear wave splitting using S and SKS phases can often be compared to and explained by strains generated by past and present geological processes [Silver and Chan, 1988, 1991]. We apply the method of Silver and Chan [1991] to 186 well-recorded SKS and S wave arrivals and obtain 135 direct measurements of the fast polarization azimuth (ϕ) and delay time (δt) as well as 51 null results (Table A3). Null results may indicate either the absence of anisotropy or that the back azimuth is equal to ϕ or $\phi \pm \pi/2$. Observations from a range of back azimuths can resolve this ambiguity.

The SKS phase is shown for one event from the coast of California recorded at 8 of the 11 stations (Figure 2). There is clear evidence of shear wave splitting in the existence of tangential energy on the theoretically radially polarized SKS phase. For waves traveling through an isotropic media, particle motion should remain predominantly rectilinear, whereas shear wave splitting, due to anisotropy, will produce more elliptical

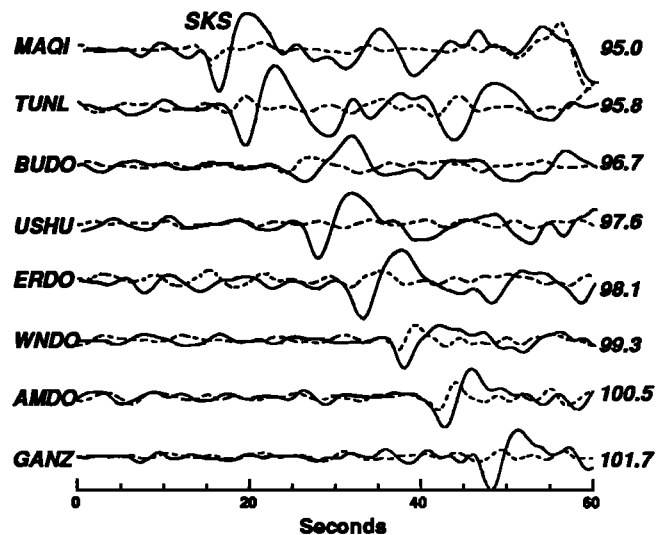


Figure 2. The SKS phase is shown for event 91.229.19.45.21. Solid line is the radial component of motion, and the dashed line shows tangential motion. Distance in degrees from the event to the recording station is indicated at the right of each trace. The existence of energy on the tangential component of motion is a possible indication of shear wave splitting.

particle motion. Systematic variations in this shear wave splitting with event back azimuth are evidence that it has resulted from shear velocity anisotropy. The method of *Silver and Chan* [1991] uses a grid search technique to determine the ϕ and δt that best remove the effects of anisotropy. This is done by observing which combination of ϕ and δt most successfully minimizes the *SKS* energy on the tangential component, or in the case of direct *S*, best linearizes the particle motion.

To prepare the original seismograms for analysis, we cut a 150-s window around the International Association of Seismology and Physics of the Earth's Interior (IASPEI) [Kennett and Engdahl, 1991] predicted arrival time of the phase of interest and decimated the data to 20 samples/s. LHAS was an exception since data were originally recorded at 5 samples/s. We then visually inspected the data and selected a window around one cycle of well-recorded impulsive *SKS* or *S* phases. We show stages of the analysis procedure using the event from Figure 2 recorded at AMDO (back azimuth=27°, $\Delta=100.5^\circ$) (Figure 3).

In the radial-tangential coordinate system, energy is apparent on the tangential component, and the waveform shape resembles the derivative of the radial component (Figure 3a) as expected for splitting [Silver and Chan, 1991]. The existence of elliptical particle motion indicates strong off-azimuth energy for a normally radially polarized arrival (Figure 3b). The grid search resulted in a *SKS* phase with a delay time of 0.9 s when rotated to a coordinate system defined by $\phi=65^\circ$ (Figure 3c). Energy is significantly reduced on the corrected tangential component when a 0.9-s shift is applied in the fast azimuth coordinate system (Figure 3e). In addition the corrected particle motion is significantly linearized (Figure 3f).

In order to assess the uncertainty of each measurement, a contour plot of energy on the corrected tangential component is plotted as a function of all (ϕ , δt) pairs (Figure 3d). The actual (ϕ , δt) estimate is shown as a star within the 95% confidence region. In the absence of detectable splitting or when ϕ is either parallel or perpendicular to the back azimuth, δt is

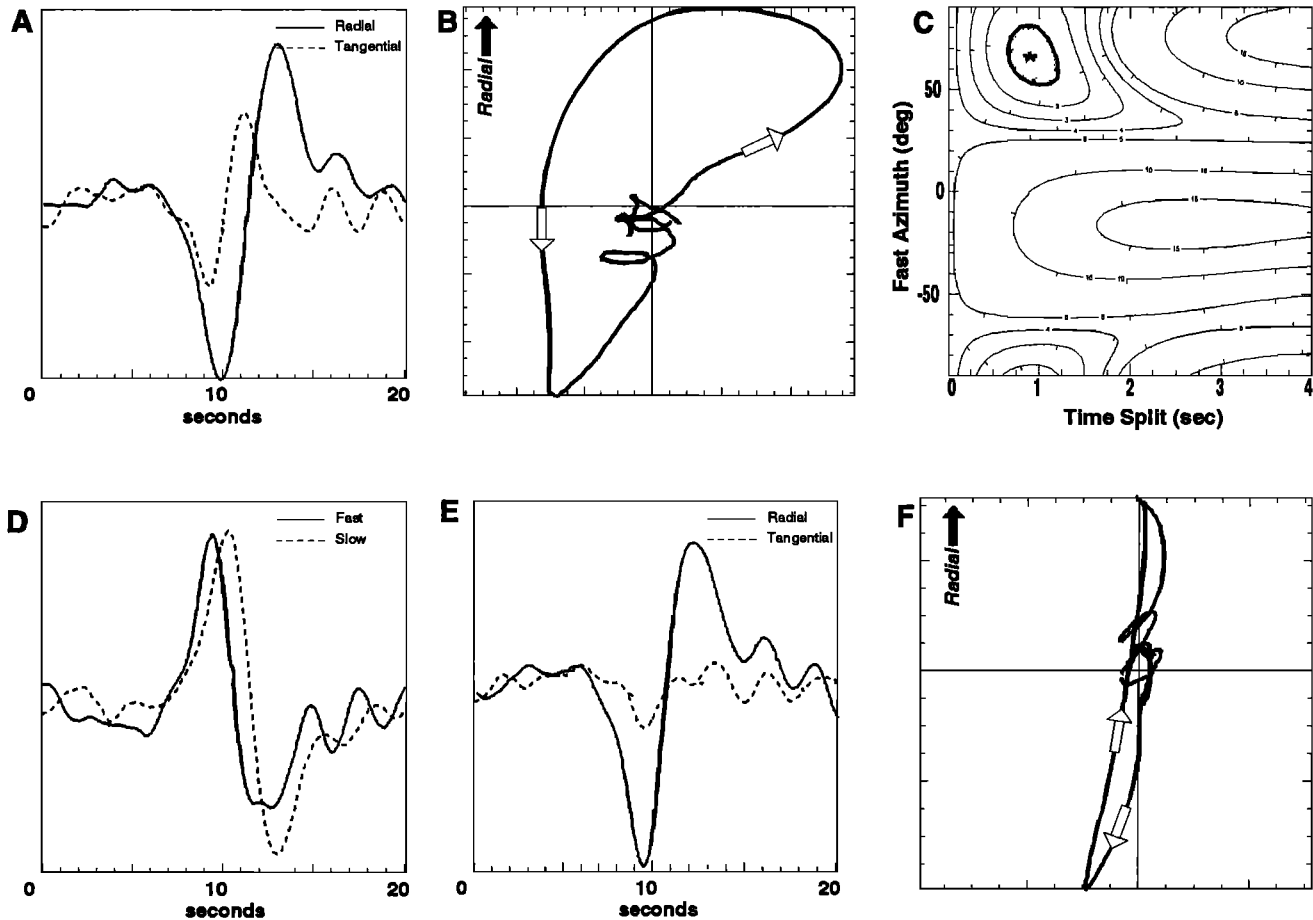


Figure 3. The anisotropy analysis procedure is pictured using event 91.229.19.45.21 from near the coast of California recorded at AMDO (back azimuth=27°, $\Delta=100.5^\circ$). (a) *SKS* phase in the radial-tangential coordinate system. Energy is apparent on the tangential component whose waveform shape resembles the derivative of the radial component. (b) Elliptical particle motion of the original *SKS* phase in the radial/tangential coordinate system. There is strong off-azimuth energy for the normally radially polarized *SKS* phase. (c) Contour plot of energy on the corrected *SKS* tangential component computed through the entire range of (ϕ , δt). Minimum value is indicated by a star at ($\phi=65^\circ$, $\delta t=0.9$ s) along with 95% confidence region shown within the bold contour in gray. (d) *SKS* rotated to fast-slow coordinate system. *SKS* phase has a split time δt of 0.9 s when rotated to a coordinate system defined by a fast azimuth ϕ of 65°. (e) Corrected *SKS* in radial-tangential coordinate system. A 0.9-s shift was applied to the slow component in the fast-slow coordinate system. The seismograms, which were then rotated back to the radial/tangential coordinate system, show that energy on the tangential component of motion is reduced. (f) Resultant linear particle motion of corrected *SKS* phase in the radial-tangential coordinate system.

unconstrained. These cases can be identified when energy function contours are elongate in δt and do not show a clear minimum. This indicates that either the phase has arrived along the fast or slow polarization direction or the anisotropy is very weak. We have considered results to be null when they produce this type of energy contour. We include these results in Table A3 because the event back azimuths may be an indication of either the fast or slow azimuth of anisotropy [Silver and Chan, 1991].

Results

We made measurements at all stations with sufficiently impulsive and isolated *SKS* and *S* phases using 46 different events. These results are tabulated in Table A3 and plotted as straight lines in rose diagrams in Figure 4. Note the well-defined grouping of observations at each station and the variation in both ϕ and δt from station to station. These results demonstrate that both fast polarization direction and delay time vary across the array. Seven of the 11 stations have a sufficient number of *SKS* observations so that no *S* wave measurements

are included in the final results (Figure 4). The remaining four stations (GANZ, LHSA, USHU, XIGA) are deficient in measurable *SKS* splitting for a variety of reasons. USHU and LHSA have only null results, while GANZ and XIGA have only two and one nonnull results, respectively (Table A3). This indicates that the fast or slow direction of anisotropy at these stations is parallel to the back azimuth direction of events from the *SKS* source regions of the South Pacific and California. The paucity of *SKS* observations at GANZ and XIGA is also a result of the nearly 40% station downtime discussed earlier [Owens *et al.*, 1993a].

In order to enhance the reliability of our anisotropy measurements, especially at stations with few *SKS* observations, impulsive *S* waves with observed elliptical particle motion are also examined using the technique of Silver and Chan [1991]. Initially, only events deeper than 50 km with epicentral distances from 40° to 75° were selected because we were interested in only well-isolated and steeply incident *S* wave arrivals. In some cases, measured splitting parameters (ϕ , δt) matched *SKS* results well. However, in most cases, measurements of ϕ and δt from direct *S* varied significantly (Figures 5a and 5b).

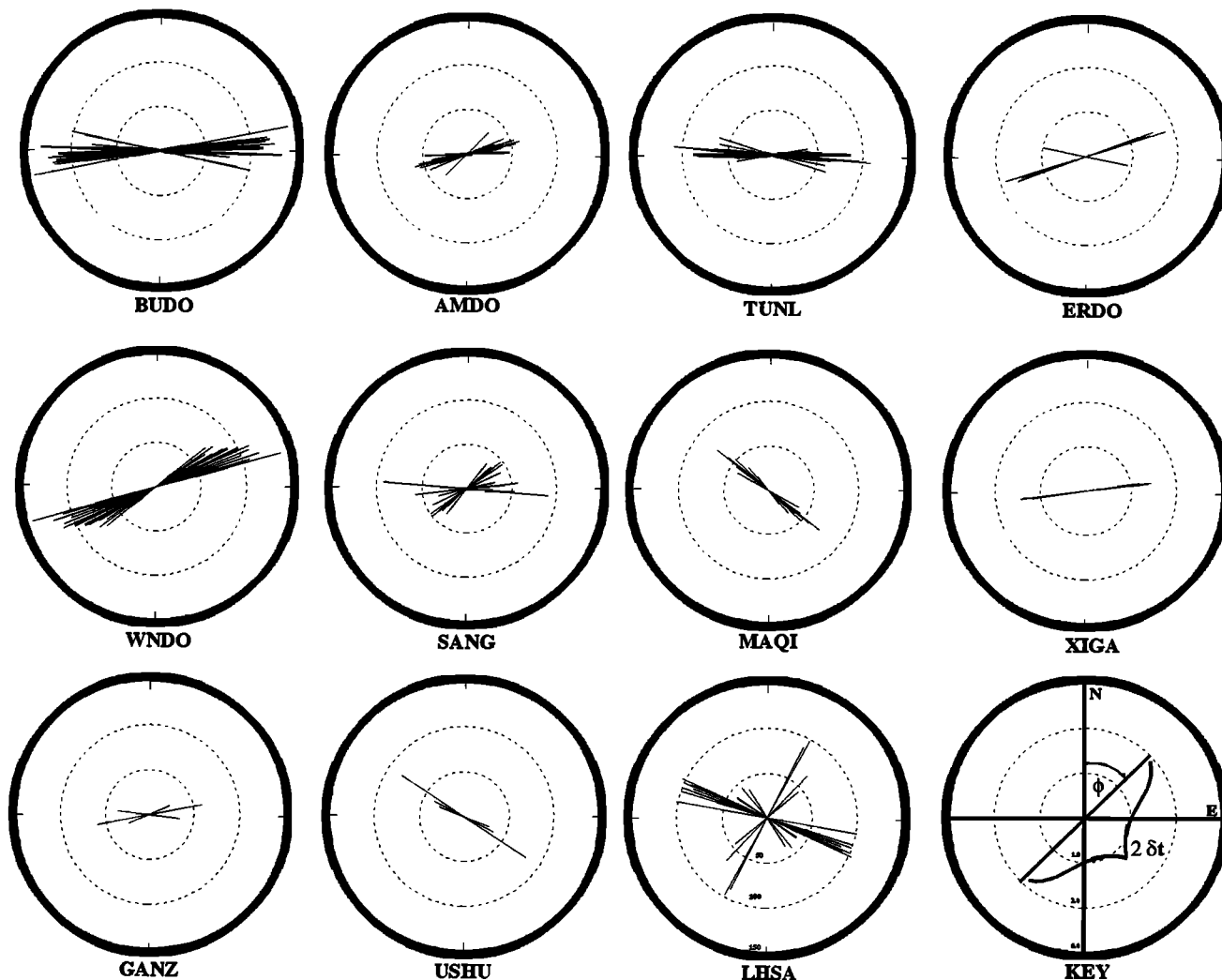


Figure 4. Results of the anisotropy measurements of shear wave splitting by station. Fast azimuths ϕ and split times δt for *S* and *SKS* phases are plotted on rose diagrams for 10 stations. δt increases outward from 0 to 3 s. Back azimuths and epicentral distances of null results are shown for LHSA. For LHSA only, orientations indicate the event back azimuth; half line lengths indicate the event distance in degrees. For all other plots, see lower right diagram for a key.

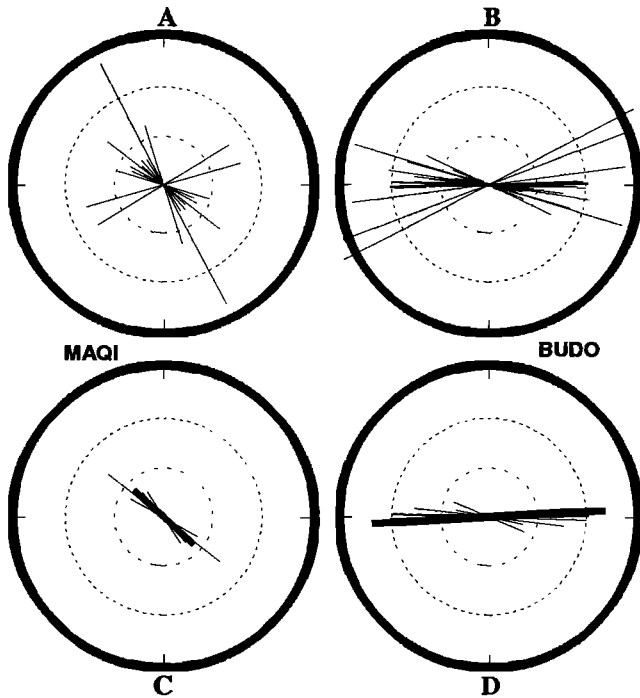


Figure 5. Source-side anisotropy and its effect on shear wave splitting measurements. Fast azimuths, ϕ , and split times, δt , are plotted for two stations (MAQI, BUDO) in a rose diagram. δt increases outward from 0 to 3 s. (a) All nonnull results at MAQI. (b) All nonnull results at BUDO. (c) Results for events with focal depths greater than 200 km at MAQI. The thick solid line represents the average SKS splitting parameters measured at MAQI. (d) Results for events with focal depths greater than 200 km at BUDO. The thick solid line represents the average SKS splitting parameters measured at BUDO. Note the consistency of the S wave results, from deep events, with the SKS results in Figure 4.

Unlike SKS, shear wave splitting of direct S can be a result of anisotropic regions at both the source and receiver ends of the ray path. Kaneshima and Silver [1992] have used similar observations to suggest that source side splitting may be a feature of shallow to intermediate depth subduction zone earthquakes. To test if S wave splitting parameter variation could be influenced by source side anisotropy, we eliminated shallow to intermediate depth events (depth < 200 km) from S wave splitting results at MAQI and BUDO, which both have ample SKS observations (Figures 5c and 5d). Scatter is reduced, and consistency with the results from our SKS observations is increased when we include only events with depths greater than 200 km, suggesting that receiver side anisotropy is the most significant component of splitting for deep events. Source side anisotropy from the active subduction zones of the western Pacific appears to complicate direct S arrivals from shallow earthquakes. We have therefore eliminated these shallow events and only included 32 S waves from events with focal depths greater than 200 km in the measurements of receiver side anisotropy beneath the Tibetan Plateau (Table A3). Although peripheral to this study, these results also suggest that the nature of the source side component of anisotropy could be investigated using the direct S wave arrivals once receiver side anisotropic parameters are clearly defined.

Average polarization direction of fast shear waves (ϕ) and time delay between the fast and slow shear waves (δt) at each station are calculated from the nonnull measurements using the computed error as a weight (Table A3). For the seven stations with a sufficient number of SKS observations, averages are computed only using SKS measurements (Table 1 and Figure 4). The addition of S wave results to our averaging has increased the number of observations at both GANZ and XIGA by only one measurement. For this reason, resultant values of ϕ and δt at these stations are less constrained than the remainder of the array. In support of these measurements is the fact that back azimuths from several null S and SKS observations are consistent with the measurements of ϕ and δt (Table A3). Two well-constrained S wave measurements of ϕ and δt and one moderate quality measurement were obtained at USHU. Measurements of ϕ at USHU are consistent, although values of δt vary slightly. The two best constrained measurements indicate a small amount of splitting ($\delta t=0.6-0.75$) (Table A3 and Figure 4). The third measurement of δt is larger by more than a factor of 2 but has an error 15 to 30 times larger than the well-constrained results. This indicates that splitting at USHU is most likely small. Even with the addition of S wave observations, no non null measurements were obtained at LHSA. Since the back azimuth of results are an indication of either the fast or slow direction, null event back azimuth and distances are plotted in place of ϕ and δt for LHSA (Figure 4). Though not reported, mean splitting parameters calculated for the seven stations with ample SKS estimates remained stable with the addition of S waves results.

There are several interesting features in the averaged splitting parameters that deserve interpretation. Most obvious is the variation of ϕ and δt from station to station despite the consistency of results at each station. Resulting estimates of the fast polarization direction ϕ and delay time δt show systematic variation along the north-south line (Figures 1 and 6). The lines plotted at each station in Figure 1 and 6 have orientations corresponding to the estimated fast azimuth, ϕ , and lengths corresponding to the measured value of δt . Note the systematic rotation of ϕ from about 50° (NE) to 90° (E-W) from south to north along the line. We observe very large delay times at three stations at the northern end of the array. The largest SKS splitting ever recorded (2.4 s) is observed toward the northern edge of the plateau at BUDO (Figures 1 and 6 and Table 1). However, just off the northern edge of the plateau at TUNL (110 km from BUDO), δt drops to only 0.93 s. Sites in the south central plateau (AMDO, SANG) also exhibit splitting much smaller than BUDO, ERDO, and WNDO.

Table 1. Tibetan Plateau Experiment Results (Station Averages)

| Station | ϕ , deg | δt , s |
|---------|-----------------|-------------------|
| TUNL | 88.8 | 0.93 |
| BUDO | 86.7 | 2.40 |
| ERDO | 73.4 | 1.49 |
| WNDO | 62.0 | 1.91 |
| AMDO | 75.0 | 0.88 |
| SANG | 51.0 | 0.80 |
| LHSA* | 120.0 | --- |
| XIGA† | 81.5 | 1.25 |
| GANZ† | 79.0 | 0.94 |
| MAQI | 131.8 | 0.82 |
| USHU‡ | 119.0 | 0.72 |

* No splitting observed with ϕ in null direction.

† Average computed with SKS and S .

‡ Average computed with only S waves.

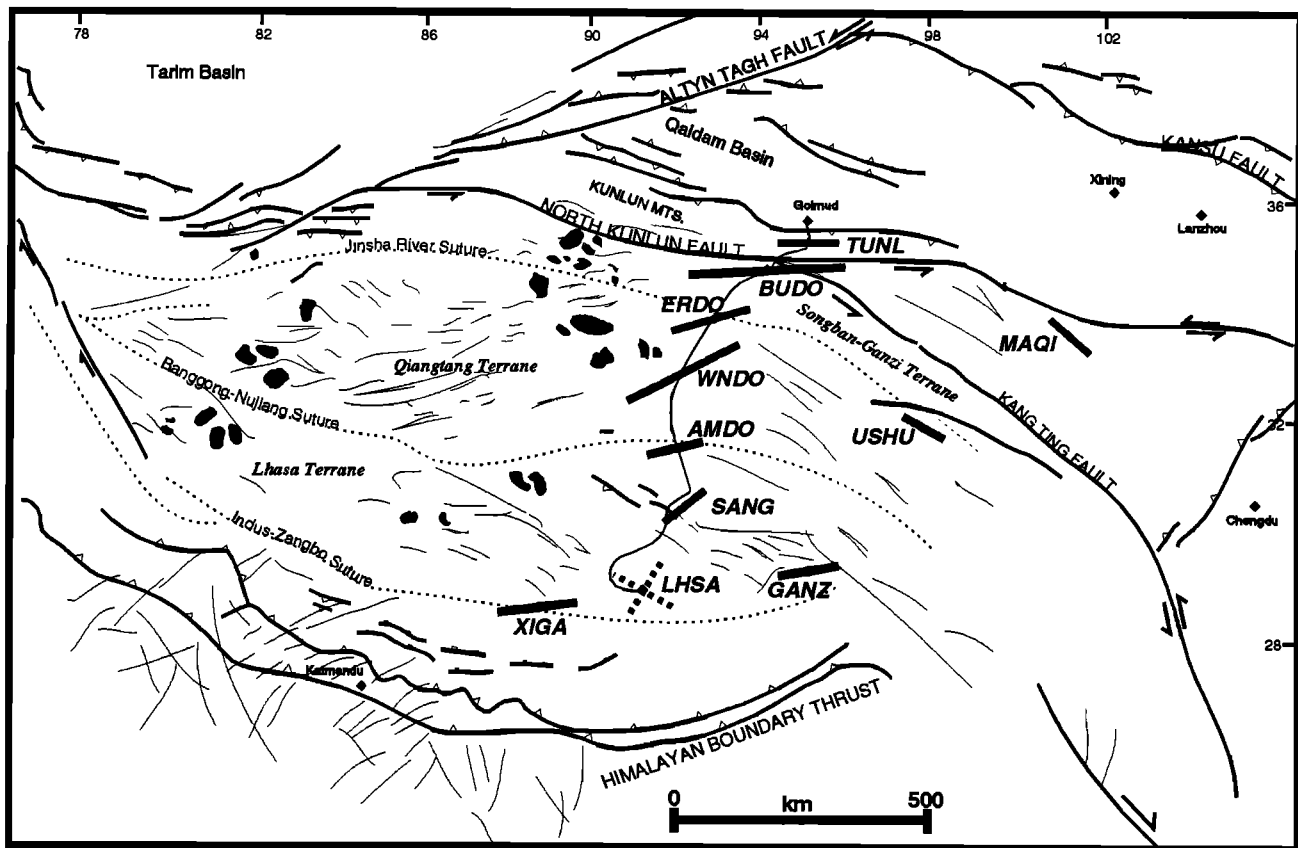


Figure 6. Tibetan Plateau map with major faults, sutures and terranes [after Dewey *et al.*, 1988]. Resultant anisotropy parameters, plotted at each station, show the correlation to local tectonic features. Lineaments within the plateau represent strike-slip fault traces and dark regions show the location of recent volcanics.

Discussion

Localization of anisotropy. The near-vertical ray path of *SKS* provides excellent lateral resolution of mantle anisotropy. On the other hand, at a single station, depth resolution is poor because, in principle, anisotropy could be anywhere along the final leg of the *SKS* path from the core-mantle boundary to the surface. The use of a network of stations is advantageous because the relatively tight receiver spacing allows for better depth constraints. We have observed variations in splitting results among closely spaced stations within our array which is an indication that the source of shear wave splitting cannot be deep in the mantle. For example, while BUDO and TUNL are only separated by 110 km, δt varies by nearly a factor of 3 (Table 1). At each site, the source of anisotropy must be directly beneath the station, within a cone-shaped volume, whose base is at the core-mantle boundary with a radius of approximately 1500 km [Silver and Chan, 1991]. Our observation that BUDO and TUNL have dissimilar results means that the anisotropic regions must be outside a region defined by the intersection of their two cones and, therefore, in the upper mantle and/or crust. In addition, a deep mantle source is unlikely because, below the mantle transition zone, the mantle appears to be isotropic [Kaneshima and Silver, 1992; Silver *et al.*, 1993].

Further constraints can be placed on the depth to the source of anisotropy by determining the crustal component of anisotropy. The crust beneath the Tibetan Plateau is known to be

anomalously thick (~70km). If velocity anisotropy were restricted exclusively to the crust, then even in the case of a 70-km-thick crust, we would require abnormally high values of anisotropy to produce the large values of δt observed in our *SKS* and *S* data set. However, we can assess the crustal contribution of anisotropy beneath the array by analysis of the Moho *Ps* phase. Previous studies have shown that since the *Ps* phase is converted from a *P* to an *S* wave at the Moho, it is a good means of constraining crustal anisotropy [McNamara and Owens, 1993].

We searched the data for high signal to noise radial *Ps* phases in source-equalized receiver functions [Zhu *et al.*, 1993a,b]. We evaluated over 1800 receiver functions and found only 25 Moho *Ps* phases with either elliptical particle motion, energy on the tangential component of motion, or evidence of measurable splitting between the horizontal components of motion. Four of the 11 stations had no evidence of splitting (ERDO, MAQI, XIGA, SANG). Five stations showed weak evidence of splitting (AMDO, BUDO, TUNL, WNDQ, USHU), and one station recorded numerous impulsive Moho *Ps* arrivals with measurable splitting (GANZ).

Using the methods of McNamara and Owens [1993] we determined ϕ and δt from split *Ps* arrivals for six of the 11 stations. Crustal shear wave fast polarization directions measured with *Ps* at five stations (AMDO, BUDO, TUNL, WNDQ, USHU) were consistent with those obtained using *SKS*. Average measurements of δt range from 0.26 s at TUNL to 0.17 s at BUDO. As mentioned, few measurable Moho *Ps* phases were found, so these results are not well constrained.

Only GANZ recorded a sufficient number of measurable split P_s phases to be considered reliable. We examined 121 receiver functions and found 12 with measurable shear wave splitting. An average fast polarization direction of $\phi=36^\circ$ and a split time of $\delta t=0.19$ s was obtained at GANZ. The fast polarization direction measured from SKS at GANZ is roughly 45° from the crustal fast azimuth. This suggests that the measured SKS split time of 0.94 s does not accurately reflect anisotropy in the mantle beneath GANZ. It is interesting to note that very few reliable SKS and direct S splitting measurements were obtained at GANZ. This may be a result of multiple anisotropic layers complicating the waveform [Savage and Silver, 1993; Silver and Savage, 1993].

Splitting measurements obtained from SKS and direct S are many (4 to 14) times larger than δt measured from the Moho P_s phase. This would suggest that while crustal anisotropy may have an effect on SKS and direct S splitting, it certainly does not dominate our results. Though few P_s observations were available, at five of six stations it appears that ϕ in the crust and mantle are coupled and have a similar effect on shear wave splitting. P_s delay times are small relative to SKS , so the anisotropy in the crust alone cannot account for our observed delay times. A split time of less than 0.25 s will not have any effect on the longer period SKS phase [Silver and Chan, 1991]. As previously stated, the variation in splitting parameters (ϕ , δt) across the array enables us to rule out a lower mantle anisotropy source. Thus, we can conclude that the source of a majority of our observed splitting in the SKS and direct S phases is a region of velocity anisotropy in the upper mantle.

Anisotropic layer modeling: Thickness and composition. If we assume that the observed splitting is from a single layer of anisotropic material, its apparent thickness can be approximated by

$$L = \frac{\delta t \beta_o}{\delta \beta}$$

where δt is the measured shear phase split time, β_o is the isotropic shear velocity of the layer, and $\delta \beta$ is the coefficient of anisotropy or fractional difference in velocity between the fast and slow azimuths [Silver and Chan, 1988, 1991]. For our modeling, we select $\beta_o = 4.7$ km/s, which we obtained from published S_n propagation velocities for the mantle lid beneath the Tibetan Plateau [Chen and Molnar, 1981]. To constrain $\delta \beta$, we must make several assumptions. First, we assume that anisotropy is due to the preferred orientation of mantle minerals since the alignment of cracks can be ruled out at these depths. Second, we assume olivine is the anisotropic mineral causing our observed splitting since it is the most abundant and most anisotropic mineral present in the upper mantle. Olivine in syn-tectonically recrystallized aggregates tends to be oriented with the short axis ([010] direction) parallel to the maximum shortening direction and the long axis ([100] direction) parallel to extension extension [Christensen, 1984]. The maximum single-crystal shear wave anisotropy in olivine is $\delta \beta=17\%$ with values of $\delta \beta=10\%$, 7% , and 2% for propagation along [001], [010], and [100], respectively. These values of $\delta \beta$, however, are significantly reduced in naturally occurring peridotites. For dunites, or the olivine fraction of peridotite samples, $\delta \beta$ from petrofabric measurements are roughly half the single-crystal values [Christensen and Lundquist, 1982; Mainprice and Silver, 1993]. Assuming $\beta_o=4.7$ km/s and $\delta \beta=4\%$, a range of thicknesses from 94 km (SANG, $\delta t=0.8$ s) to 282 km (BUDO, $\delta t=2.4$ s) is required if we must account for our split times by

thickness variations alone. The thickness pattern across the northern plateau is interesting for two reasons. First, computed anisotropic layers for these stations are thicker than the remainder of the array, although we observe considerable local variation between stations (BUDO=282 km, ERDO=175 km, WNDO=224 km). Second, there are strong thickness transitions at the boundaries of this region. To the north, from BUDO to TUNL, computed thickness decreases by 172 km. To the south, from WNDO to AMDO, computed thickness decreases by 121 km. Thus, by assuming a conventional anisotropy coefficient for peridotites ($\delta \beta=4\%$) we find anisotropic layer thicknesses that may extend well into the mantle. Since such extreme thicknesses and abrupt thickness variations seem geologically unrealistic. Rather than simply the thickness of the anisotropic layer varying across the array, $\delta \beta$ may be affected by localized variations in the degree of the preferred orientation of olivine crystals in the mantle beneath each station. Also, varying the crustal contribution, though relatively small, could cause variations in δt [Barroul and Mainprice, 1993].

The north central Tibetan Plateau is particularly interesting because of the large amount of seismic data that can be interpreted as evidence for high temperatures in the upper mantle. For example, inefficient S_n propagation [Ni and Barazangi, 1983; Beghoul et al., 1993], large teleseismic $S-P$ travel time residuals [Molnar and Chen, 1984; Molnar, 1990], and slow Rayleigh phase velocities [Brandon and Romanowicz, 1986] can all be interpreted as evidence for anomalous heat production in this portion of the plateau. The seismic evidence is supported by geologic evidence observed at the surface. In the northern Tibetan Plateau there is strong evidence for widespread Cenozoic volcanism with both basaltic and granitic components [Deng, 1978; Dewey et al., 1988; Molnar et al., 1987; Molnar, 1988] (Figure 6). The basaltic composition suggests volcanic sources from partial melt of upper mantle material.

The correlation of our large δt observations with other evidence for a hot upper mantle under the north central Tibetan Plateau leads to an alternative to associating larger δt with thicker anisotropic zones. If the upper mantle is hot, weak, and perhaps partially melted, then this may allow for more efficient alignment of olivine crystals. An end-member interpretation of an anisotropic layer of constant 100 km thickness would have $\delta \beta = 3.8\%$ at SANG and $\delta \beta = 11\%$ at BUDO. Such high values of splitting ($\delta \beta = 11\%$) are, however, uncommon in the upper mantle. Even for the most deformed mantle samples, $\delta \beta$ is not expected to be any greater than about 8% for pure olivine [Mainprice and Silver, 1993]. Thus we infer at least some variation in thickness of the anisotropic upper mantle in the northern plateau. In any case, our observations require a very rapid change in the properties of the upper mantle across the North Kunlun front (between BUDO and TUNL) as well as internal variations within the northern Tibetan Plateau (Figure 6).

Tectonic source of anisotropy. Interpretations of shear wave splitting in terms of tectonic and geologic processes involves relationships between splitting and anisotropy, between anisotropy and strain, and finally between strain and tectonic processes. Reasonable assumptions can be made about all three of these relationships so that it is possible to use the predicted splitting properties of various hypotheses to test which may be applicable to the Tibetan Plateau (see Silver and Chan [1991] for details). There are two probable processes for the origin of upper mantle anisotropy within continental interiors. The first is

the internal coherent deformation of the continental lithosphere (ICL [Silver and Chan, 1991]) by the latest significant deformation episode. In presently stable regions, this would correspond to "fossil anisotropy" left over from the last tectonic episode, whereas in presently active areas, the episode would be the present one. This hypothesis would predict a close correspondence between the strains inferred from surface geologic/tectonic features and those inferred from the anisotropic properties of the upper mantle. Second, the anisotropy could result from absolute plate motion (APM) of the Tibetan Plateau with respect to the ambient mantle below. In this case, ϕ should be parallel to the APM direction of the Tibetan Plateau. Unfortunately, Eurasia is moving so slowly that the actual APM direction is not well constrained. In any case, this hypothesis would predict that splitting properties should be slowly varying over the plate, and can be tested on this basis.

Figure 6 is a summary of detailed maps presented by Dewey *et al.*, [1988]. We have included the major thrust and strike-slip faults of the region. These features tend to trend roughly east to west, aligning closely with the fast polarization direction measured at stations in the north, south, and east of the array (BUDO, TUNL, MAQI, USHU, XIGA, GANZ). The east-west trace of the North Kunlun front runs directly between TUNL and BUDO then turns southward to parallel fast polarization directions at USHU and MAQI (Figure 6). The most striking features of the splitting results are the close alignment of the fast polarization direction with the fault and the extreme variation in the amount of delay time across the fault. This strongly suggests that the North Kunlun fault is a major tectonic feature whose influence extends well into the upper mantle. The North Kunlun fault marks the northern boundary of the Tibetan Plateau. The variation of δt between TUNL and BUDO suggests that there are significant variations of mantle properties across this zone.

To the south, XIGA and GANZ show good alignment with major east-west trending suture zones and currently active thrust faults of the Himalaya (Figure 6). This is expected if strain is producing splitting with the fast polarization direction orthogonal to the direction of collision between the northward advancing Indian plate and the Eurasian plate. The remaining four stations (ERDO, WNDO, AMDO, SANG) in the central portion of the array have weak correlations with the trend of geologic fabric and strike-slip lineations in the central Tibetan Plateau (Figure 6).

Inferred seismic anisotropy and models of the Tibetan Plateau. Our shear wave anisotropy observations are an additional constraint on mechanical models of this region. Using the ICL theory presented by Silver and Chan [1991], we argue that the results presented here can be explained best by upper mantle deformation that is coherent with the current surface deformation of the Tibetan Plateau. The apparent correlation of ϕ (an indicator of coherent strain in the mantle) with surface geologic fabric and crustal anisotropy parameters (indicators of the present collisional deformation) will need to be explained by any viable tectonic model. In addition, our results suggest a much thicker layer of upper mantle anisotropy or an increased efficiency of mineral alignment in the north central plateau. The primary significance of these data lie in their use as constraints on the strain field produced by deformation during a collisional event. For the Tibetan Plateau, most models eventually invoke catastrophic removal of the mantle lithosphere and replacement with hot asthenosphere [Beghoul *et al.*, 1993; England and Houseman, 1989]. Now such models must

explain the correlation between surface and mantle deformation.

Since earth scientists first speculated about the formation of the Tibetan Plateau, underthrusting of the Indian continent beneath the Eurasian continent, in some manner, has been discussed in the scientific literature [Argand, 1924; Powell and Conaghan, 1973; Zhao and Morgan, 1987]. Most recently, Beghoul *et al.* [1993] have proposed a "modified" hydraulic pump model. Hydraulic uplift occurs due to underthrusting and injection of the Indian lithosphere into the soft Tibetan Plateau mantle lid. Their modification has the leading edge of the Indian plate advanced northward, only 2/3 the length of the plateau. The northern 1/3 of the plateau is not yet underthrust by India and is being thinned by either a delamination or thermal erosion process. This model implies that asthenospheric material flows upward to replace the lithospheric mantle lid beneath the north central Tibetan Plateau.

In support of the Beghoul *et al.* [1993] model, we do observe a rapid change in the anisotropy parameters in the northern plateau. It is also difficult to argue with certainty whether the observations at XIGA, GANZ, and LHASA are associated with "Indian" or "Tibetan" mantle lithosphere. However, their model implies vertical asthenospheric flow beneath the north central Tibetan Plateau. Because vertical flow would lead to negligible shear wave splitting (assuming the a axis of olivine is parallel to the flow) it is difficult to reconcile this with large shear wave splitting of near vertically incident waves and apparent correlation of ϕ with surface geologic fabric.

A second class of models that have been proposed to explain the anomalous nature of the Tibetan Plateau, suggests that enough stress is generated by the collision of the Indian and Eurasian plates to deform the plateau by "distributed shortening" [e.g. Dewey and Bird, 1970; Houseman *et al.*, 1981]. The expected characteristics of a plate deformed in this manner would be a thickened crust with a thickened, low-temperature, high seismic velocity lithospheric mantle. While these models predict crustal properties, predicted mantle properties are inconsistent with a wide range of geophysical data suggesting a thin mantle lid. Distributed shortening models thus must be modified. This is generally accomplished by removal of cold sub-continental mantle material through some form of convective instability. Warm buoyant material from the asthenosphere replaces the colder and denser lithosphere as it delaminates from the crust [England and Houseman, 1989]. These models are also difficult to reconcile with our splitting results. Very little is known about the strain field associated with this sort of asthenospheric flow pattern, though it would be surprising that it would be similar to geologic trends at the surface.

Complicating both classes of models is the contribution of lateral, eastward, extrusion of Tibetan Plateau continental blocks in response to the collision [Tapponnier *et al.*, 1990]. Harrison *et al.* [1992] suggest that at least one third of shortening can be accounted for by lateral extrusion. Upper mantle deformation in response to lateral extrusion of continental blocks along the east-west oriented strike slip faults should produce strong anisotropy with fast polarization directions parallel to the faults and the direction of extrusion. Measurements of shear wave splitting along the San Andreas fault have produced strong delay times (1.2 s) and a fast polarization direction parallel to the trend of the fault [Savage *et al.*, 1990; Barroul and Mainprice, 1993]. Similarly, we observe shear wave fast polarization directions nearly parallel to the Kunlun fault zone at several stations (MAQI, USHU, TUNL, BUDO) (Figure 6). Continental extrusion of the Tibetan Plateau may also explain

the large difference in δt between TUNL and BUDO as well as the similarity of ϕ . As the Tibetan Plateau block extrudes eastward, flow may be induced in the hot upper mantle, efficiently aligning olivine crystals, increasing $\delta\beta$, and causing large values of δt . Conversely, the relatively colder fixed block north of the Kunlun fault may not experience the same level of deformation in the mantle lid as beneath BUDO. Therefore weaker mineral alignment would result in smaller values of $\delta\beta$ and δt . The current strain field across the Tibetan Plateau predicts the existence of extrusion tectonics along major strike-slip faults, and it is interesting to note that our splitting results show a rotation across the plateau that is similar to the strain rate field obtained from summed moment tensors [Holt and Haines, 1993].

Our observations of large splitting with fast polarization directions that parallel geologic trends at the surface might also suggest lithospheric-wide deformation in which heating of the mantle occurred in place without removal and replacement of asthenospheric material. Silver and Chan [1991] have suggested a means of both heating the upper mantle lid and deforming it coherently with the remainder of the lithosphere. If orogenic stresses resulting from the collision between the Indian and Eurasian plates are large enough, then as the mechanical work of shortening is converted to heat, the upper mantle lid could be sufficiently heated and deformed in place. The critical issue in this argument is the actual level of orogenic stresses. Silver and Chan [1991] require that several hundred megapascals of stress be generated during the collision to produce the appropriate temperature increase in the Tibetan Plateau mantle lid. A wide range of mantle strengths and stresses have been reported to be associated with the formation and evolution of the Tibetan Plateau (20–600 MPa) [Bird, 1978; Cloetingh and Wortel, 1986; McAdoo and Sandwell, 1985; England and Houseman, 1986, 1989; Molnar and Lyon-Caen, 1988]. The high end of this range would be sufficient to produce the "in situ" heating of the lithosphere, in place, required by Silver and Chan [1991].

To test the viability of strain heating, a more accurate accounting of the available stresses will be needed. If cumulative stress levels are high enough (several hundred megapascals) and the crust and mantle deform coherently, it may in fact be possible to explain the elevated temperatures of the subcontinental mantle by some form of strain induced heating. This would allow for strain in the upper mantle lithosphere to be coherent with the surface in the presence of elevated temperatures.

Conclusions

We have analyzed shear wave splitting from the mantle beneath the central and eastern Tibetan Plateau in an attempt to place useful constraints on the nature of the tectonic evolution of the plateau. Significant observations include the following: individual station measurements of ϕ vary smoothly from north to south across the central Tibetan Plateau; and some of the largest values of splitting ever measured at stations are located within a previously identified zone of inefficient S_n propagation in the north central Tibetan Plateau.

The coherence of many of our directions of fast polarization with surface geological features suggests that a significant portion of the subcontinental mantle is involved in the collisional deformation that has produced the Tibetan Plateau. Existing models for the evolution of the Tibetan Plateau do not provide

enough quantitative information about the predicted strain field in the mantle for us to test these models in a rigorous manner. We suggest, however, that it will be difficult for models involving catastrophic removal of the mantle lithosphere to produce correspondence between deformation at the surface and the top few hundred kilometers of the mantle. Further quantitative predictions are clearly needed. We also suggest that models for in situ deformation of the mantle lithosphere including some mode of strain heating should also be carefully considered in light of the correlation between the mantle and surface deformation.

Acknowledgments. This experiment was a cooperative project with the Institute of Geophysics, State Seismological Bureau, People's Republic of China through the research group of R.S. Zeng. Chinese participants included Z. Zeng, Z. Deng, W. Sun, Z. He, and L. Zhu. This project also benefited from the hard work and cooperation of scientists from the Seismological Bureau of the Qinghai Province and the Tibetan Autonomous Region. In addition to the authors, many people contributed to the success of the experiment by traveling to China during the year of deployment. U.S. participants in the field program included R. Busby (PIC-LDEO), R. Kuenel (Carnegie-DTM), G. Randall, G. Wagner, S. Owens, and M. Salvador (USC). The PASSCAL Instrument Center at Lamont-Doherty Earth Observatory provided considerable support during the year. A complete data report and all data collected during the experiment are now available through the data management center at IRIS. This project was supported by NSF grants EAR-9004428 EAR-9196115 and EAR-9206815 to USC and EAR-9004221 to SUNY at Binghamton. Denise Apperson provided considerable advice on early versions of this paper. Comments by X. R. Shih and an anonymous reviewer helped improve our presentation and interpretation.

References

- Argand, E., La tectonique de L'Asie, *Proc. 13th Geol. Congr. Brussels*, 13, 170–372, 1924.
- Barazangi, M., and J. Ni, Velocities and propagation characteristics of P_n and S_n beneath the Himalayan arc and Tibetan Plateau: Possible evidence for underthrusting of Indian continental lithosphere beneath Tibet, *Geology*, 10, 179–185, 1982.
- Barroul, G., and D. Mainprice, A quantitative evaluation of the contribution of crustal rocks to the shear wave splitting of teleseismic SKS waves, *Phys. Earth Planet. Inter.*, 78, 281–300, 1993.
- Beghoul, N., M. Barazangi, and B. L. Isacks, Lithospheric structure of Tibet and western North America: Mechanisms of uplift and a comparative study, *J. Geophys. Res.*, 98, 1997–2016, 1993.
- Bird, P., Initiation of intracontinental subduction in the Himalaya, *J. Geophys. Res.*, 83, 4975–4987, 1978.
- Brandon, C., and A. Romanowicz, A "No-lid" zone in the central Chang-Thang platform of Tibet: Evidence from pure path phase velocity measurements of long-period Rayleigh waves, *J. Geophys. Res.*, 91, 6547–6564, 1986.
- Chen, W. P., and P. Molnar, Constraints on seismic wave velocity structure beneath the Tibetan Plateau and their tectonic implications, *J. Geophys. Res.*, 86, 5937–5962, 1981.
- Christensen, N. I., and S. M. Lundquist, Pyroxene orientation within the upper mantle, *Geol. Soc. Am. Bull.*, 93, 279–288, 1982.
- Christensen, N. I., The magnitude symmetry and origin of upper mantle anisotropy based on fabric analysis of ultramafic tectonites, *Geophys. J. R. Astron. Soc.*, 76, 89–111, 1984.

- Cloetingh, S., and R. Wortel, Stress in the Indo-Australian plate, *Tectonophysics*, 132, 49–67, 1986.
- Deng, W., A preliminary study on the petrology and petrochemistry of the Quaternary volcanic rocks of the Northern Tibet Autonomous region, *Acta. Geol. Sin., Engl. Transl.*, 52, 148–152, 1978.
- Dewey, J. F., and J. M. Bird, Mountain belts and the new global tectonics, *J. Geophys. Res.*, 75, 2625–2647, 1970.
- Dewey, J. F., and K. C. A. Burke, Tibetan, Variscan, and Precambrian basement reactivation: Products of continental collision, *J. Geol.*, 81, 683–692, 1973.
- Dewey, J. F., R. M. Shackleton, F. R. S. Chang Cheng, and S. Yiyin, The tectonic evolution of the Tibetan Plateau, *Philos. Trans. R. Soc. London.*, 327, 379–413, 1988.
- England, P. C., and G. Houseman, Finite strain calculations of continental deformation, 2, Comparison with the India-Asia collision zone, *J. Geophys. Res.*, 91, 3664–3676, 1986.
- England, P. C., and G. Houseman, Extension during the continental convergence, with application to the Tibetan Plateau, *J. Geophys. Res.*, 94, 17,561–17,579, 1989.
- Harrison, T. M., P. Copeland, W. S. F. Kidd, and A. Yin, Raising Tibet, *Science*, 255, 1663–1670, 1992.
- Hess, H., Seismic anisotropy of the uppermost mantle under oceans, *Nature*, 203, 629–631, 1964.
- Holt, W. E., and A. J. Haines, Velocity fields in deforming Asia from the inversion of earthquake-released strains, *Tectonics*, 12, 1–20, 1993.
- Houseman, G. A., D. P. McKenzie, and P. Molnar, Convective instability of a thickened boundary layer and its relevance for the thermal evolution of continental convergence belts, *J. Geophys. Res.*, 86, 6115–6132, 1981.
- Kaneshima, S., and P. G. Silver, A search for source side mantle anisotropy, *Geophys. Res. Lett.*, 19, 10,048–10,052, 1992.
- Kennett, B., and E. Engdahl, Travel times for global earthquake location and phase identification, *Geophys. J. Int.*, 105, 429–465, 1991.
- Mainprice, D., and P. G. Silver, Interpretation of *SKS* using samples from the subcontinental lithosphere, *Phys. Earth Planet. Inter.*, 78, 257–280, 1993.
- McAdoo, D. C., and D. T. Sandwell, Folding of oceanic lithosphere, *J. Geophys. Res.*, 90, 8563–8569, 1985.
- McNamara, D. E., and T. J. Owens, Azimuthal shear wave velocity anisotropy in the Basin and Range Province using Moho *Ps* converted phases, *J. Geophys. Res.*, 98, 12,003–12,017, 1993.
- Molnar, P., *S*-wave residuals from earthquakes in the Tibetan region and lateral variations in the upper mantle, *Earth Planet. Sci. Lett.*, 101, 68–77, 1990.
- Molnar, P., A review of geophysical constraints on the deep structure of the Tibetan Plateau, the Himalaya and the Karakoram, and their tectonic implications, *Trans. R. Soc. London., Ser. A*, 327, 33–88, 1988.
- Molnar, P., and W. P. Chen, *S*-*P* travel time residuals and lateral inhomogeneity in the mantle beneath Tibet and the Himalaya, *J. Geophys. Res.*, 89, 6911–6917, 1984.
- Molnar, P., and H. Lyon-Caen, Some physical aspects of the support, structure, and evolution of mountain belts, *Mem. Geol. Soc. Am.*, 218, 178, 1988.
- Molnar, P., B. C. Burchfiel, Z. Zhao, K. Liang, S. Wang, and M. Huang, Geological evolution of northern Tibet: Results of an expedition to Ulugh Muztagh, *Science*, 235, 299–305, 1987.
- Ni, J., and M. Barazangi, High frequency seismic wave propagation beneath the Indian shield, Himalayan arc, Tibetan Plateau and surrounding regions: High uppermost mantle velocities and efficient propagation beneath Tibet, *Geophys. J. R. Astron. Soc.*, 72, 665–689, 1983.
- Nicolas, A., and N. I. Christensen, Formation of anisotropy in upper mantle peridotites—A Review, in *Composition, Structure and Dynamics of the Lithosphere-Asthenosphere System, Geodyn. Ser.*, vol. 16, edited by K. Fuchs and C. Froidevaux, pp. 111–123, AGU Washington D.C., 1987.
- Ozalaybey, S., and M. K. Savage, Double layer anisotropy resolved from *SKS* waveforms, *J. Geophys. Jour.*, in press, 1994.
- Owens, T. J., G. E. Randall, F. T. Wu, and R. S. Zeng, PASSCAL instrument performance during the Tibetan Plateau passive seismic experiment, *Bull. Seismol. Soc. Am.*, 83, 1959–1970, 1993a.
- Owens, T. J., G. E. Randall, D. E. McNamara, and F. T. Wu, Data Report for the 1991-92 Tibetan Plateau passive-source seismic experiment, *PASSCAL Data Rep. #93-005*, IRIS, Wash. DC, 1993b.
- Powell, C. M., and P. J. Conaghan, Plate tectonics and the Himalayas, *Earth Planet. Sci. Lett.*, 20, 1–12, 1973.
- Savage, M. K., and P. G. Silver, Mantle deformation and tectonics: Constraints from seismic anisotropy in the western United States, *Phys. Earth Planet. Inter.*, 78, 207–227, 1993.
- Savage, M. K., W. A. Peppin, and U. R. Vetter, Shear-wave anisotropy and stress direction in and near Long Valley Caldera, California, *J. Geophys. Res.*, 95, 11,165–11,177, 1990.
- Silver, P. G., and W. W. Chan, Implications for continental structure and evolution from seismic anisotropy, *Nature*, 335, 34–39, 1988.
- Silver, P. G., and W. W. Chan, Shear wave splitting and sub-continental mantle deformation, *J. Geophys. Res.*, 96, 16,429–16,454, 1991.
- Silver, P. G., S. Kaneshima, and C. Meade, Why is the lower mantle so isotropic?, *Eos Trans. AGU*, 74(16), Spring Meeting suppl., 313, 1993.
- Silver, P. G., and M. K. Savage, The interpretation of shear-wave splitting parameters in the presence of two anisotropic layers, *Geophys. J. Int.*, in press, 1994.
- Tapponnier, R., R. Lacassin, P. H. Leloup, U. Scharer, Zhong D., Wu H., Liu X., Ji S., Zhang L., and Zhong J., The Ailao Shan/Red River metamorphic belt: Tertiary left-lateral shear between Indochina and South China, *Nature*, 343, 431–437, 1990.
- Windley, B. F., Tectonic framework of the Himalaya, Karakoram and Tibet, and problems of their evolution, *Philos. Trans. R. Soc. London., Ser. A*, 326, 3–16, 1988.
- Zhao, W., and J. Morgan, Injection of Indian crust in to Tibetan lower crust: A two-dimensional finite element model study, *Tectonics*, 6, 505–514, 1987.
- Zhou, L., D. V. Helmberger, and D. G. Harkrider, Shear-velocity of the crust and upper mantle beneath the Tibetan Plateau and southeastern China, *Geophys. J. Int.*, 105, 713–730, 1991.
- Zhu, L., R. Zeng, F. T. W., T. J. Owens, and G. E. Randall, Preliminary study of crust-upper mantle structure of the Tibetan Plateau by using broadband teleseismic body waveforms, *Acta Seismol. Sin.*, 6, 305–316, 1993a.
- Zhu, L., T. J. Owens, and G. E. Randall, Lateral variation in crustal structure of the northern Tibetan Plateau inferred from teleseismic receiver functions, *Eos Trans. AGU*, 74(43), Fall Meeting Suppl., 425, 1993b.

D. E. McNamara and T. J. Owens, Department of Geological Sciences, University of South Carolina, Columbia, SC 29208. (e-mail: dem; owens@tiger.seis.scarcolumbia.edu)

P. G. Silver, Department of Terrestrial Magnetism, Carnegie Institution of Washington, 5241 Broad Branch Rd., N.W., Washington, DC 20015. (e-mail: silver@pssl.ciw.edu)

F. T. Wu, Department of Geological Sciences, SUNY at Binghamton, Binghamton, NY 13902-6000. (e-mail: wu@sunquakes.geol.binghamton.edu)

(Received May 26, 1993; revised November 22, 1993; accepted November 30, 1993.)